ZANCO Journal of Pure and Applied Sciences
The official scientific journal of Salahaddin University-Erbil
https://zancojournals.su.edu.krd/index.php/JPAS

ISSN (print):2218-0230**, ISSN (online):** 2412-3986**, DOI: http://dx.doi.org/10.21271/zjpas**

RESEARCH PAPER

New schiff base ligand type [LH2] donor derevative from 4-Aminophenol with Manganese (II), Cobalt(II), Nickal(II), and Copper(II)

Shaee Asaad Shahbahram , Iman Ibrahim Abdulkareem

Koya University /Faculty of science and health / Chemistry department

A B S T R A C T:

The condensation reaction between dimethylglyoxime, acetic acid, and 4-aminophenol was significantly influenced by the [LH_2] type donor derivative ligand. The reaction was conducted in methanol for 24 hours while being stirred and refluxed. The syntheses forming a new (*2E,3E)-butane-2,3-dione O2-((E)-1-((4-hydroxyphenyl)imino)ethyl) O3-((Z)-1-((4-hydroxyphenyl)imino)ethyl*) *dioxime)* dioxime ligand type [LH_2]. Spectroscopic techniques (FT-IR and UV-Vis), elemental analysis (CHN), magnetic susceptibility testing, thin-layer chromatography (TLC), X-RD powder diffraction, ^{1}H-NMR molar conductance, and other methods have been used to characterize the ligand and its complexes with the general formula [$M(LH_2)$] where [M= Mn(II), Co(II), Ni(II), and Cu(II), and [LH_2] = donor atoms ligand with N_4 and O]. Our study reveals the formation of a new ligand and new complexes with trigonal bipyramid geometrical shape around the Manganese(II), Cobalt(II), Nickel(II), and Copper(II) metal ions. Biological function using the agar disc diffusion method for the ligand and its complexes showed considerable activity against one kind of bacteria (*Staphylococcus aureus*) after being exposed to two types of bacteria *(Staphylococcus aureus and Escherichia coli*).

KEY WORDS: 4-aminophenol, dimethylglyoxime, acetic acid, five-coordinate trigonal bipyramidal complex, Schiff bases.
DOI: http://dx.doi.org/10.21271/ZJPAS.35.1.18
ZJPAS (2023) , 35(1);177-188 .

1.INTRODUCTION :

Due to their capacity for forming stable complexes with the majority of transition metals. Coordination chemistry has benefited from the development of Schiff bases. Chemistry has been studying the intriguing structural variations of Schiff base ligand species extensively (Asadi et al., 2011) (Monfared et al., 2011) (Chamayou et al., 2011). Amines can attack electrophilic carbon atoms in aldehydes and ketones by nucleophilic assault. This reaction produces a molecule with a C=N double bond in place of a C=O double bond. The usual formula for this kind of molecule, an imine or Schiff base, is $R_1R_2C=NR_3$, where R is an organic side chain. Azomethine and Schiff base are interchangeable in this definition. Several Schiff base complexes have remarkable catalytic activity in a range of processes and in the presence of moisture (Abu-Dief and Mohamed, 2015).

In the last decade Schiff base ligands have received more attention mainly because of their wide applications in the field of catalysis and due to their antimicrobial and antifungal activity(Lamani et al., 2009).

The aim of the study

Is to prepare a new derivative donor ligand type [LH_2] and its complexes in the form of crystal with some metal ions, and characterizing them by

* **Corresponding Author:**
Shaee Asaad Shahbahram
E-mail: Shayi.asaad@koyauniversity.org
Article History:
Received: 04/08/2022
Accepted: 10/09/2022
Published: 20/02 /2023

spectroscopic methods and testing them with two positive and negative bacteria.

Materials

The chemical reagents dimethylglyoxime, acetic acid, 4-aminophenol, methanol, ethanol, commercially available and used without purification were manganese(II) acetate tetrahydrate, cobalt(II) acetate tetrahydrate, nickel(II) acetate tetrahydrate, and cupric(II) acetate monohydrate. Just before use, solvents were extracted from the proper drying agents.

Physical Measurements

On a Buchi melting point B-540 melting point equipment, melting points were achieved. In the 4000-400 cm^{-1} range, Fourier transform infrared (FT-IR) spectrophotometer data were collected. Using an Agilent Technologies spectrophotometer with a quartz cell of (1.0 cm) length, the visible wavelengths of the produced compounds were measured in the range 200-800 nm in dimethyl sulfoxide (DMSO) at 25 ^{0}C. Analyses of the elements were done on a (CHN). Using a TDS&EC Temperature digital conductivity meter, electrical conductivity measurements of the complexes were taken for 10^{-6} M solutions of the samples in methanol at room temperature. Following Faraday's approach, magnetic susceptibility measurements were taken at room temperature. Using a (BRUKER 400 CRYOPROBE) spectrometer, the proton one-nuclear magnetic resonance (^{1}H-NMR) spectra for DMSO-d^6 solutions was obtained. The X-RD power diffraction of complexes was obtained using PANalytical in the range of 2^θ (0^0-60^0).

Synthesis and characterization of derivative Ligand type [LH_2].

In two phases, the [LH_2] derivative ligand was made from the reaction of dimethylglyoxime and acetic acid to form carbonyl compound and by adding the 4-aminophenol according to the general route shown in scheme (1). The prepared compound was obtained in (81%), and characterized by spectroscopic methods. As in the following: -

Step – 1 synthesis of carbonyl compound

Dimethylglyoxime (2 g, 17.2 mmol) in a combination with (40 ml) of methanol was stirred and heated until a clear solution formed, and (2 ml, 34.4 mmol) of acetic acid was added to it, and leave to stand for reflux for (24 hrs.) in a 100 ^{0}C, white color (carbonyl compound) precipitate was formed (1.13 g), (yield 56.5%), mp 244-245 ^{0}C.

Step – 2

(18 ml) of methanol and (0.43 g, 2.14 mmol) of the (carbonyl compound) was stirred and heated until a clear solution formed, and (0.46 g, 4.2 mmol) of 4-aminophenol dissolved in (20 ml) of D.W by heating was added to it, and leave to stand for reflux for (24 hrs.) in a 100 ^{0}C, dark brown color precipitate was formed (0.35 g), (yield 81%), mp 199-200 ^{0}C.

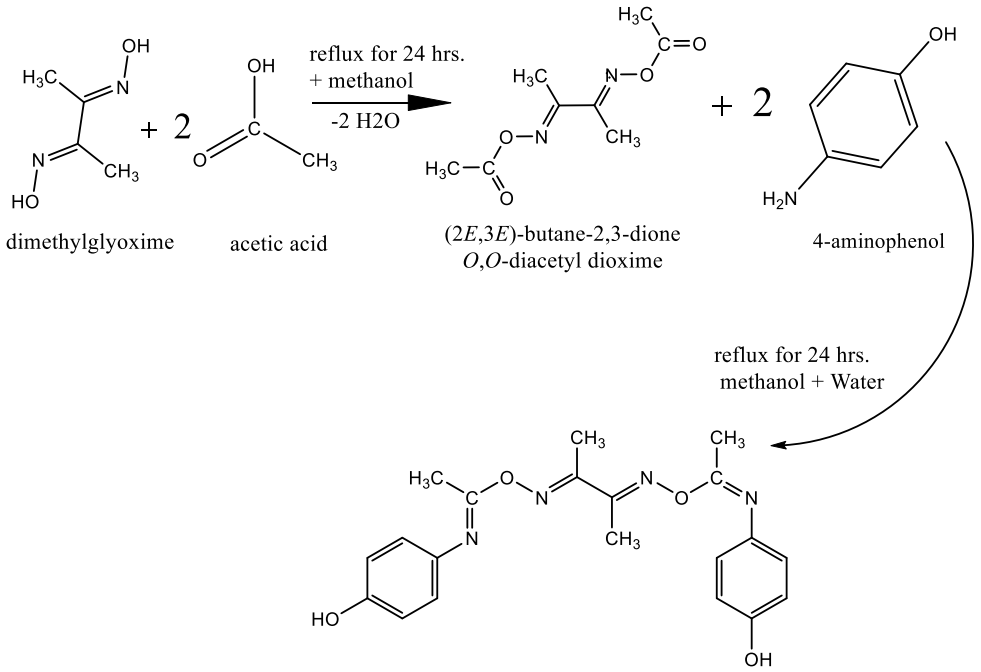

Scheme 1 preparation route of derivative ligand [LH_2] type

Syntheses of [LH_2] complexes

Syntheses of [$Mn(LH_2)$] complex

(20 ml) of ethanol was added to (0.2 g, 0.52 mmol) [LH_2]and agitated until a clear solution formed and (0.128 g, 0.52 mmol) of [$Mn(CH_3CO_2)_2 \cdot 4H_2O$] manganese(II) acetate tetrahydrate dissolved in (15 ml) of ethanol was added to it, and leave to stand for reflux for (4 hrs.) in a (100 ^{0}C) and a brown color solution was formed. (0.12 g), (yield 60%), mp 290 ^{0}C (dec.).

Syntheses of [$Co(LH_2)$], [$Ni(LH_2)$] and [$Cu(LH_2)$] complexes

The same way was used to prepare [$Mn(LH_2)$] has been used to prepare [$Co(LH_2)$], [$Ni(LH_2)$] and [$Cu(LH_2)$] complexes. Scheme (2), and all the complexes has been characterized by spectroscopic methods. Table (1) lists some of the ligand's and its complexes' physicochemical characteristics.

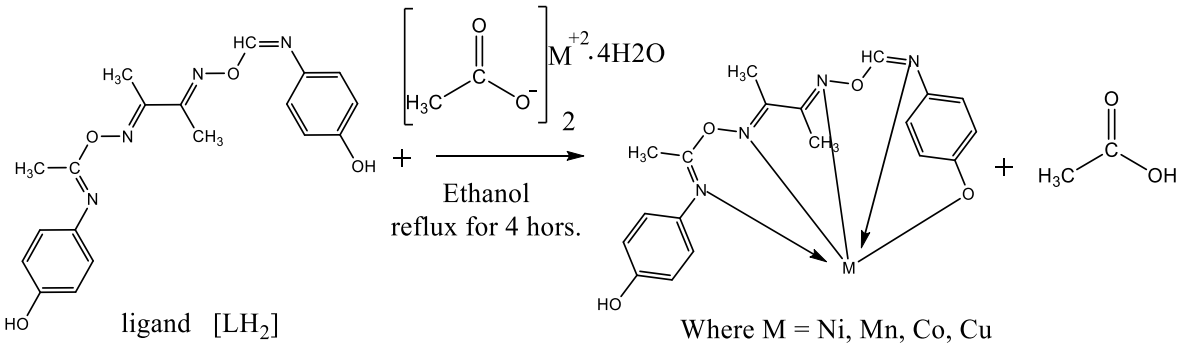

Scheme 2 preparation route of [$M(LH_2)$] complexes

Table 1 shows some physical properties for the ligand and its complexes

No.	Compound	Empirical formula	M.Wt	Yield %	m.p °C	color	Found/calculated				
							M	C	H	N	O
1	Carbonyl compound	$C_8H_{12}N_2O_4$	200.19	56.5	244-245	white	-	48.00	6.04	13.99	31.97
							-	47.47	5.32	12.87	30.32
2	[LH_2]	$C_{20}H_{22}N_4O_4$	382.42	81	199-200	Dark brown	-	62.82	5.80	14.65	16.73
							-	61.43	4.88	13.92	15.88
3	[$Mn(LH_2)$]	$C_{20}H_{21}MnN_4O_4$	436.35	60	290 (dec.)	Brown	12.59	55.05	4.85	12.84	14.67
							11.56	54.75	4.01	11.78	13.79
4	[$Co(LH_2)$]	$C_{20}H_{21}CoN_4O_4$	440.35	83	240 (dec.)	Brown	13.38	54.55	4.81	12.72	14.53
							12.90	53.77	3.67	12.00	13.80
5	[$Ni(LH_2)$]	$C_{20}H_{21}NiN_4O_4$	440.11	46	280 (dec.)	Dark brown	13.34	54.58	4.81	12.73	14.54
							12.87	53.11	3.21	11.98	13.50
6	[$Cu(LH_2)$]	$C_{20}H_{21}CuN_4O_4$	444.96	70	270 (dec.)	Dark brown	14.28	53.99	4.76	12.59	14.38
							13.88	52.66	3.89	11.87	13.77

The Ligand's FT-IR Spectrum

The band at (3196 cm^{-1}) assigned to υ(O-H) (Pimsin et al., 2021) of dimethylglyoxime figure (1-A) and the υ(O-H) at (3150 cm^{-1}) (Popescu et al., 2013) of acetic acid figure (1-B) are disappeared in the spectrum of the [LH_2] donor ligand and replaced by υ(C=N-O-C) at (977 and 1736) cm^{-1} (Pimsin et al., 2021) of the carbonyl compound figure (1-C) due to the collaboration between dimethylglyoxime and acetic acid. The υ(C=O) at (1736 cm^{-1}) (Maurya et al., 2003) of the carbonyl compound figure (1-C) and the two bands of υ(NH_2) at (3300 and 3350 cm^{-1}) (Meltzer et al., 2021) of 4-aminophenol figure (2-D) these two bands are replaced by υ(C=N) at (1691 cm^{-1})(Mondal et al., 2021) as a result of Schiff base reaction between the carbonyl compound and 4-aminophenol as shown in the figure (2-E) for the ligand [LH_2]. spectral data for the ligand and its precursors are summarized in table (2).

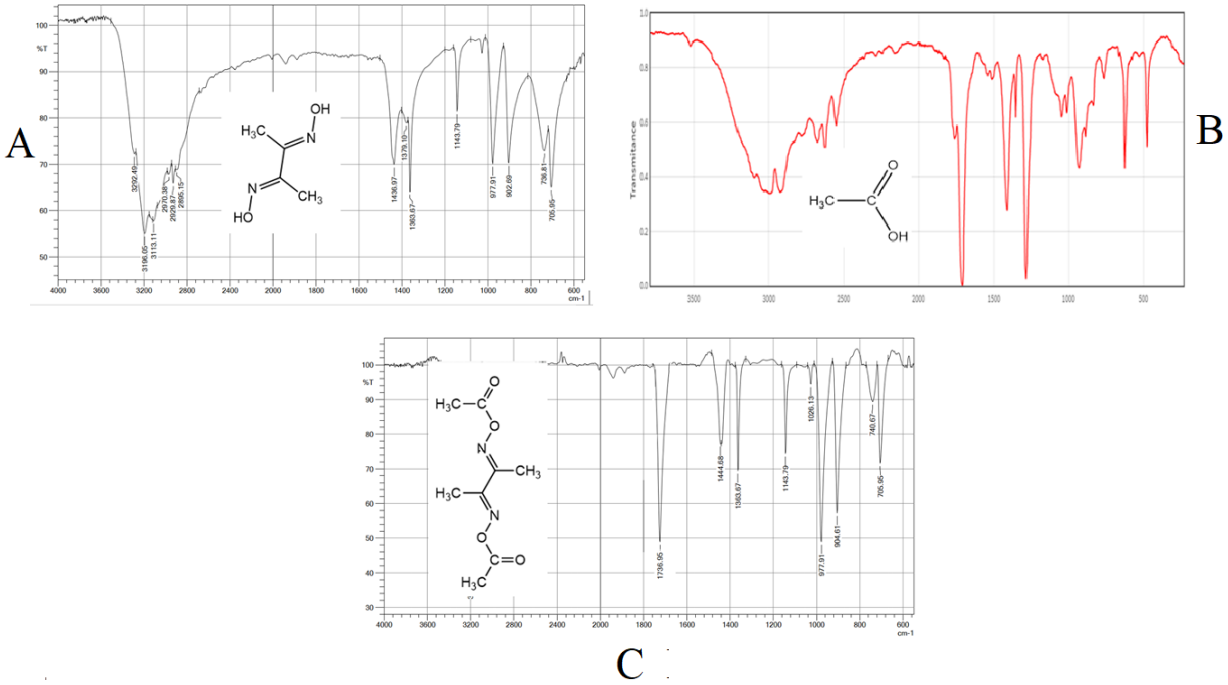

Figure 1 FT-IR Spectra of carbonyl compound and its precursors

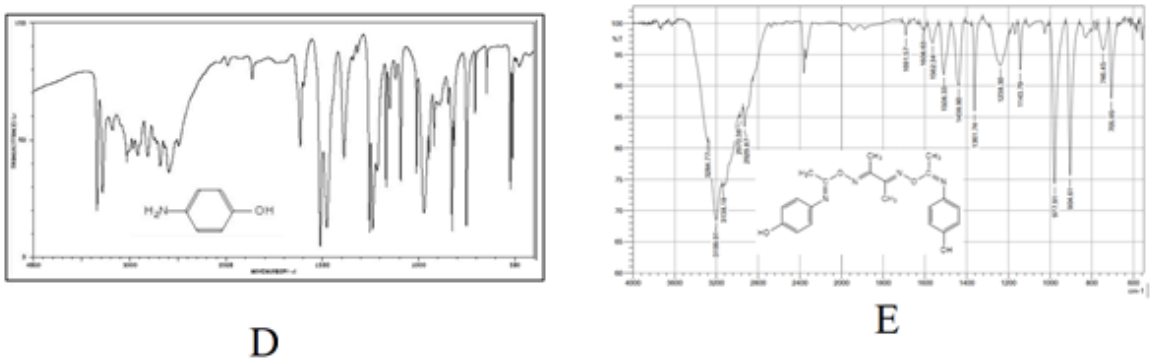

Figure 2 FT-IR Spectra of ligand [LH_2] type and its precursors

Table 2 FT-IR Spectral data for the Ligand and its Precursors

Compound	υ(N-H)	υ(O-H)	υ(C_6H_6)	υ(C=O)	υ(C=N)	υ(N-O)
dimethylglyoxime	-	3196(br)	-	-	1436 (sh)	977(sh) 1143(m)
acetic acid	-	3150(br)	-	1730(sh)	-	-
Carbonyl compound	-	-	-	1736(sh)	1444(sh)	977(sh) 1143(m)
4-aminophenol	3300(sh) 3350(sh)	3178(s)	2750(m)	-	-	-
$C_{20}H_{22}N_4O_4$ [LH_2]	-	3199(br)	2970(m)	-	1691(w)	977(sh) 1143(m)

Figures (3-F), (3-G), (3-H), and (3-I) present the FT-IR spectra of the complexes of Mn(II), Co(II), Ni(II), and Cu(II), respectively. Table(3) shows the distinguishing bands. The broadening at (3199 cm^{-1}) due to the phenol υ(O-H) (Meltzer et al.,

2021) group of the ligand [LH_2] figure (2-E), this band has been shifted to a higher frequency for the Mn(II), Co(II), Ni(II), and Cu(II)metal ion complexes at range of (3211-3221 cm^{-1}) (Mushtaque et al., 2017) in comparison to that of the free ligand, as a result of the coordination between the ligand and metal ion. The band at (2970 cm^{-1}) assign to the υ(C_6H_6) ring (Meltzer et al., 2021), and the band at (1691 cm^{-1}) of the υ(C=N) (Mondal et al., 2021) of the ligand these two bands has been shifted to a lower frequency for all the formed complexes, affected by the coordination. Furthermore, the bands at the range of (416-434 cm^{-1}) are due to υ(M-N) (Liao et al., 2001, El-Boraey et al., 2016) and (486-524 cm^{-1}) range of υ(M-O) (Liao et al., 2001, El-Boraey et al., 2016) for Mn(II), Co(II), Ni(II), and Cu(II) metal ion complexes respectively.

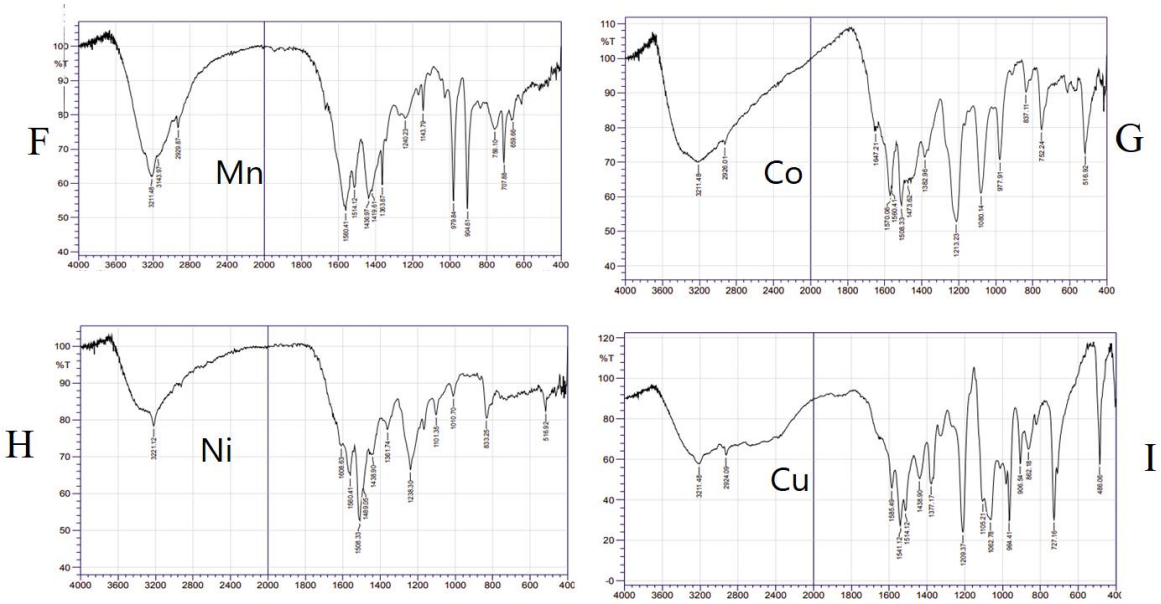

Figure 3 FT-IR spectra of Mn(II), Co(II), Ni(II), and Cu(II) metal ion complexes

Table 3 FT-IR Spectral data for the ligand and its complexes

No.	compounds	υ(O-H)	υ(C_6H_6)	υ(C=N)	υ(N-O)	υ(M-O)	υ(M-N)
1	[LH_2]	3199(br)	2970(m)	1691(w)	977(sh) 1143(m)	-	-
2	[Mn(LH_2)]	3211(br)	2929(m)	1640(w)	979(sh) 1143(m)	524(w)	430(w)
3	[Co(LH_2)]	3211(br)	2926(m)	1647(w)	977(m) 1080(m)	516(m)	416(w)
4	[Ni(LH_2)]	3221(br)	2927(m)	1608(w)	833(w) 1010(w)	516(w)	418(w)
5	[Cu(LH_2)]	3211(br)	2924(m)	1625(w)	964(sh) 1062(sh)	486(m)	434(w)

The Ligand's UV-Vis Spectrum

Figure (4-A) of the (UV-Vis) spectra for the [LH_2] derivative ligand shows a strong absorption peak at (236 nm) (38610 cm^{-1}) (ϵ_{max}=740 $molar^{-1}cm^{-1}$). Due to ($\pi \rightarrow \pi^*$) (Singh et al., 2021), with a shoulder peaks at (364 nm) (27472 cm^{-1}) (ϵ_{max}=460 $molar^{-1}$. cm^{-1}) were tasked with ($n \rightarrow \pi^*$) (Fatima et al., 2020) transition table (4).

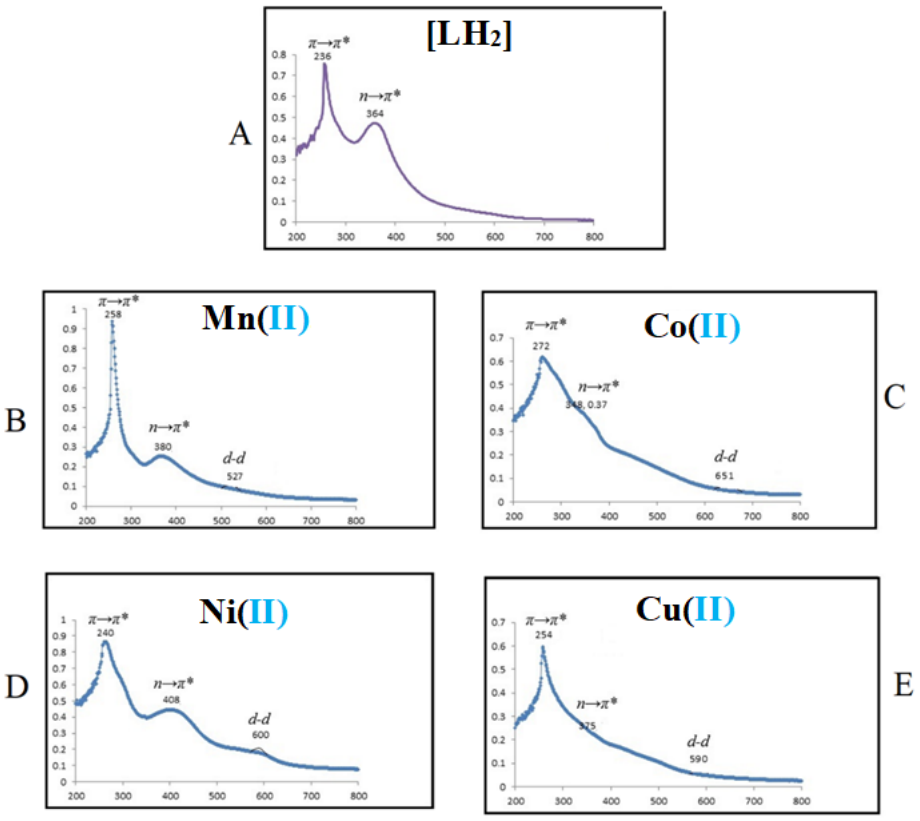

Figure 4 The UV-Vis Spectra of the [LH_2] Ligand and it's Mn(II), Co(II), Ni(II), and Cu(II) metal ion complexes

The UV-Vis Spectra of the complexes

The (UV- Vis) Spectra are shown in Figures (4-B), (4-C), (4-D), and (4-E) of Mn(II), Co(II), Ni(II), and Cu(II) complexes, respectively. Table (4) summarized the absorption peaks of the complexes. The (U.V-Vis) spectra of Mn(II), Co(II), and Cu(II) complex Figures (4-B), (4-C), and (4-E) displayed two distinct, highly pronounced absorption peaks at the range of (254-272 nm), (36764-39370 cm^{-1}), ($\in_{max}$= 460-930 $molar^{-1}. cm^{-1}$) rang assigned to the *($\pi\rightarrow\pi^*$)*(Singh et al., 2021) and (348-380 nm), (26315-28735 cm^{-1}), ($\in_{max}$= 200-370 $molar^{-1}. cm^{-1}$) rang assigned to the *($n\rightarrow\pi^*$)*(Fatima et al., 2020) ligand field for Mn(II), Co(II), and Cu(II) respectively. The third peaks at the visible region at the range of (527-651 nm), (15360-18975 cm^{-1}), ($\in_{max}$= 47-88 $molar^{-1}. cm^{-1}$) are allocated to ($^4E_g(G) \rightarrow {}^6A_{1g}$), ($^4A'_2(F) \rightarrow {}^4A'_2(P)$) and ($a'_1 \rightarrow e''$) transition, confirming trigonal bipyramidal structure around Mn(II), Co(II), and Cu(II) ion complexes (Sickerman et al., 2012). The (U.V-Vis) spectra of Ni(II) complex figure (4-D) showed two intense peaks in the range (240 nm), (41666 cm^{-1}), ($\in_{max}$= 610 $molar^{-1}. cm^{-1}$) and (408 nm), (24509 cm^{-1}), ($\in_{max}$= 440 $molar^{-1}. cm^{-1}$) rang assigned to the *($\pi\rightarrow\pi^*$)*(Singh et al., 2021) ligand field and charge transfer transition (*Ch.T*) for Ni(II). The third peak at the visible region at (600 nm), (16666 cm^{-1}), ($\in_{max}$= 160 $molar^{-1}. cm^{-1}$) is assigned to ($^2E_g \rightarrow {}^2T_{2g}$) transition, confirming trigonal bipyramidal structure around Ni(II) ion complex(Sickerman et al., 2012).

Table 4 The UV-Vis data of the [LH_2] Ligand and it's Mn(II), Co(II), Ni(II) and Cu(II) metal ion complexes

No.	Compound	υ cm^{-1}	Assignment	Geometrical shape	Ratio
1	[LH_2]	42372	$\pi\rightarrow\pi^*$		
		27472	$n\rightarrow\pi^*$		
2	[Mn(LH_2)]	38759	$\pi\rightarrow\pi^*$	trigonal bipyramidal	1;1
		26315	$n\rightarrow\pi^*$		
		18975	$^4E_g(G) \rightarrow {}^6A_{1g}$		
3	[Co(LH_2)]	36764	$\pi\rightarrow\pi^*$	trigonal bipyramidal	1;1

		28735	$n \rightarrow \pi^*$		
		15360	${}^4A'_2(F) \rightarrow {}^4A'_2(P)$		
4	$[Ni(LH_2)]$	41666	$\pi \rightarrow \pi^*$	trigonal bipyramidal	1;1
		24509	*Ch.T*		
		16666	${}^2E_g \rightarrow {}^2T_{2g}$		
5	$[Cu(LH_2)]$	39370	$\pi \rightarrow \pi^*$	trigonal bipyramidal	1;1
		26666	$n \rightarrow \pi^*$		
		16949	$a'_1 \rightarrow e''$		

^{1}H-NMR of $[LH_2]$ derivative ligand

The ^{1}H-NMR spectrum for $[LH_2]$ derivative ligand in DMSO-d^6 Fig. (5), showed singlet signal in δ (1.2 ppm) to the methyl group, the singlet signal at ppm = (2.1) was caused by methyl group of (C=N-O). The singlet signal ranged between δ (6.9-7.2 ppm) a role for the aromatic protons, and the singlet signal at δ (9.9 ppm) was due to (OH) protons indicating the exact structure of the $[LH_2]$ derivative ligand (Diab et al., 2019). While the other peaks are as in the following: - (CH_3=1.2, CH_3 of (C=N-O)=2.1, Aromatic H=6.9-9.7 and OH=9.9). (Zaki et al., 2006).

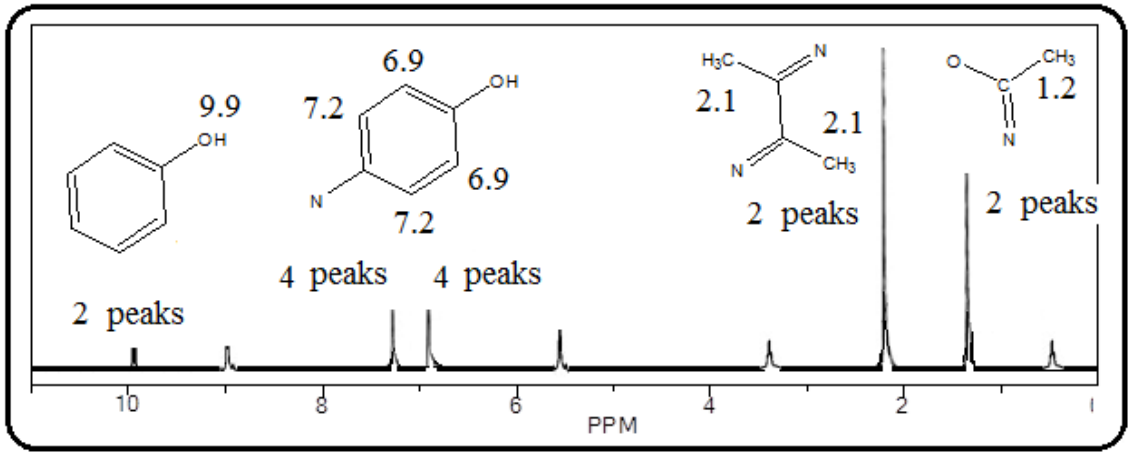

Figure 5 ^{1}H-NMR spectrum of $[LH_2]$ derivative ligand

Thin layer chromatography (TLC)

The TLC measuring method for the $[LH_2]$ derivative ligand and its complexes was performed with Mn(II), Co(II), Ni(II) and Cu(II) metal ions in a mix solution of 10 ml ethanol and 15 ml of D.W, new spots are appeared with a different *Rf* in comparison to the free ligands *Rf*. The spot positions at (2.6 cm), (1.8 cm), (3.2 cm), and (1.7 cm) of Mn(II), Co(II), Ni(II) and Cu(II) metal ion complexes respectively differ from the spot position of the $[LH_2]$ ligand at (1.4 cm) which proves the formation of the complexes as well figure (6).

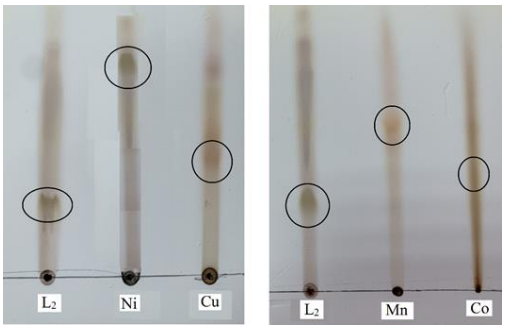

Figure 6 TLC measurements for the derivative ligand $[LH_2]$ and its complexes

Molar conductivity

The molar conductivity values of [LH_2] metal ion complexes in methanol (10^{-6} M solution) were found (18-6), these indicates that all complexes are non-electrolytic (Geary, 1971), The Molar Conductivity in (Ohm^{-1}. Cm^2. mol^{-1}) for [$Mn(LH_2)$] =18, [$Co(LH_2)$] =10, [$Ni(LH_2)$] =6 and [$Cu(LH_2)$] =10.

X-Ray power diffraction (X-RD)

The X-RD for the [LH_2] complexes figures (7) has been studied using PANalytical. At 25 °C, room temperature, all produced complexes were examined and described. During the X-RD research, the Cu K radiation was utilized for this reason. The X-RD pattern of 2θ with a range of 0° to 60° was noted. The Joint Committee for Powder Diffraction Optical Phenomena computer code (JCPDF) was used to index the X-RD pattern.)(Sharma et al., 2014). The synthesized metal complexes were characterized by X-RD measurements in order to elucidate their coordination (ligand and metal ions). To create a uniform powder, the produced complexes underwent processing steps that included washing, drying, grinding, and blending. For X-RD analyses, dry powder complexes that had been completely mixed and pulverized were employed. The d-spacing were calculated for all the produced complexes using the Bragg's equation. (Geete et al., 2020) and are given in table (5). The formula for Bragg's law is as follows: ($2d\sin\theta = n\lambda$). The d-spacing of all complexes can be compute from ^{0}2theta by the equation ($2d\sin\theta = n\lambda$) where λ= the wavelength of X-rays was 1.5406 Å and θ = the incident angle. The d-spacing is the separation between atom planes that results in diffraction peaks.

Table 5 the [^{0}2theta and d-spacing (Å)] for all complexes

[Mn(LH_2)]		[Co(LH_2)]		[Ni(LH_2)]		[Cu(LH_2)]	
^{0}2theta θ position	d-spacing [Å]	^{0}2theta θ position	d-spacing [Å]	^{0}2theta θ position	d-spacing [Å]	^{0}2theta θ position	d-spacing [Å]
23.1395	3.84391	38.487	2.33912	38.4708	2.34007	38.4677	2.33832
26.2834	3.39082	44.7106	2.02524	42.0639	2.14812	38.5724	2.338
26.5872	3.35276	44.8378	2.02481	44.716	2.02501	42.0772	2.1457
26.9764	3.30526			44.8461	2.02445	43.6211	2.07327
38.4595	2.3388			49.1528	1.8521	44.6978	2.02579
38.5675	2.33829			65.0873	1.43194	44.8313	2.02509
42.0938	2.14489			65.2734	1.43185	49.1112	1.85357
44.7159	2.02501					50.9502	1.7909
44.8441	2.02454						
49.1365	1.85267						
55.279	1.66046						

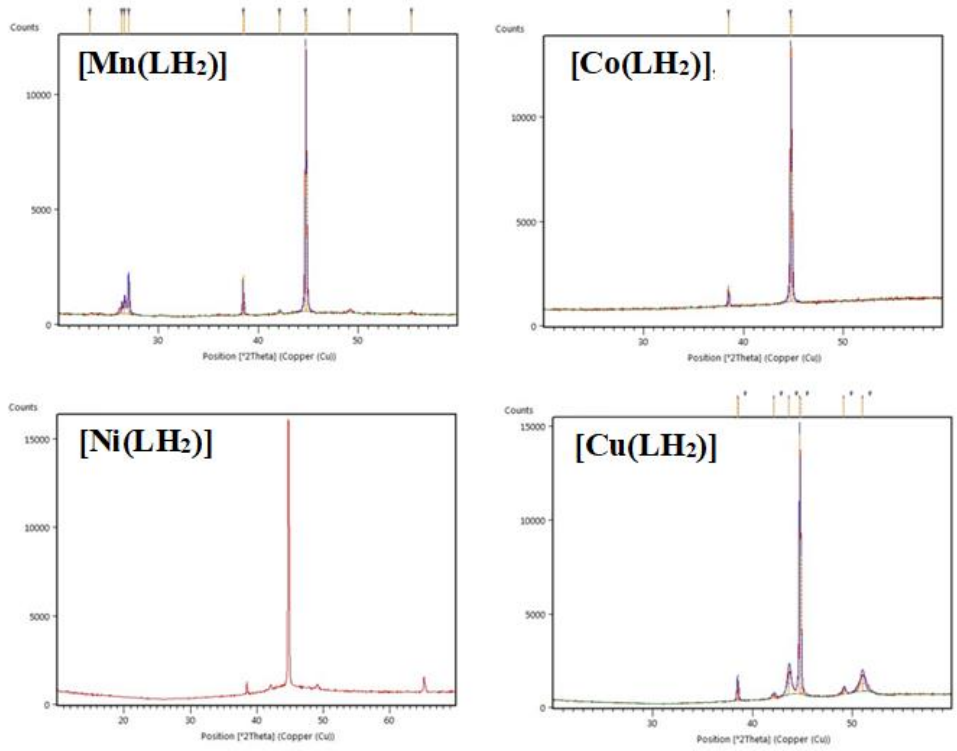

Figure 7 X-RD patterns of synthesized [Mn(LH$_2$)], [Co(LH$_2$)], [Ni(LH$_2$)] and [Cu(LH$_2$)]

Magnetic susceptibility measurements

By using Faraday's approach, the magnetic moment in the solid state has been identified. This makes it possible to count the number of unpaired electrons. Predictions of the bonding model and electrical structure should benefit from this (Bain and Berry, 2008). Table (6) shows the results of measuring the effective magnetic moment (μ_{eff} =B.M) after measuring the magnetic susceptibility of a few selected complexes at room temperature. by applying the equation $\mu_{eff} X\sqrt{2.828} = {}_{A}T$ and according to the calculated μ_{eff} it is showed that the complexes are in a high spin, the d orbital of Mn(II) have 5 unpaired electron, Co(II) have 3 unpaired electron and 2 paired electron, Ni(II) have 2 unpaired electron and 3 paired electron, Cu(II) have 1 unpaired electron and 4 paired electron, so the hybridization is sp^3d and indicating the structure of trigonal bipyramidal for all the complexes.

Table 6 data of magnetic moment (μ_{eff} of complexes (K 298) at (M.B=

No.	Complexes	Xg *10 $^{-6}$ Gram susceptibility	Xm *10^{-3} molar susceptibility	X_A *10^{-3} atom susceptibility	μ_{eff}M.B expt.	μ_{eff}M.B calc.	Suggested structure
1	[Mn(LH$_2$)]	27	11.78	11.78	5.65-6.10 1.80-2.10	5.3	Trigonal Bipyramidal
2	[Co(LH$_2$)]	10.5	4. 62	4. 63	4.30-5.20 1.8	3.32	Trigonal bipyramidal
3	[Ni(LH$_2$)]	4.5	1.98	1.99	2.80-3.50	2.17	Trigonal bipyramidal
4	[Cu(LH$_2$)]	4.5	1.99	1.9	1.70-2.20	1.97	Trigonal bipyramidal

Biological activity

Biological activity of derivative ligand [LH$_2$]

Using the inhibition approach, the biological activity of the ligand [LH$_2$] was examined in two different species of harmful bacteria. Gram

positive *Staphylococcus aureus* and gram negative *Escherichia coli* were the first two types of bacteria, respectively (Numan et al., 2015, Ibraheem et al., 2016). After 24 hours, the ligand displayed inhibition against one kind of bacterial *Staphylococcus aureus*, but not against another type of bacterial *Escherichia coli*, and this inhibitory diameter remained the same after 48 hrs., figure (8). Additionally, experiments with the same kinds of bacteria showed that the ligands exhibit greater activity than the complexes under similar experimental settings. As a standard for antibiotics Ciprofloxacin is used for gram-negative bacteria *Escherichia coli*, and Vancomycin is used for gram-positive bacteria *Staphylococcus aureus* are used.

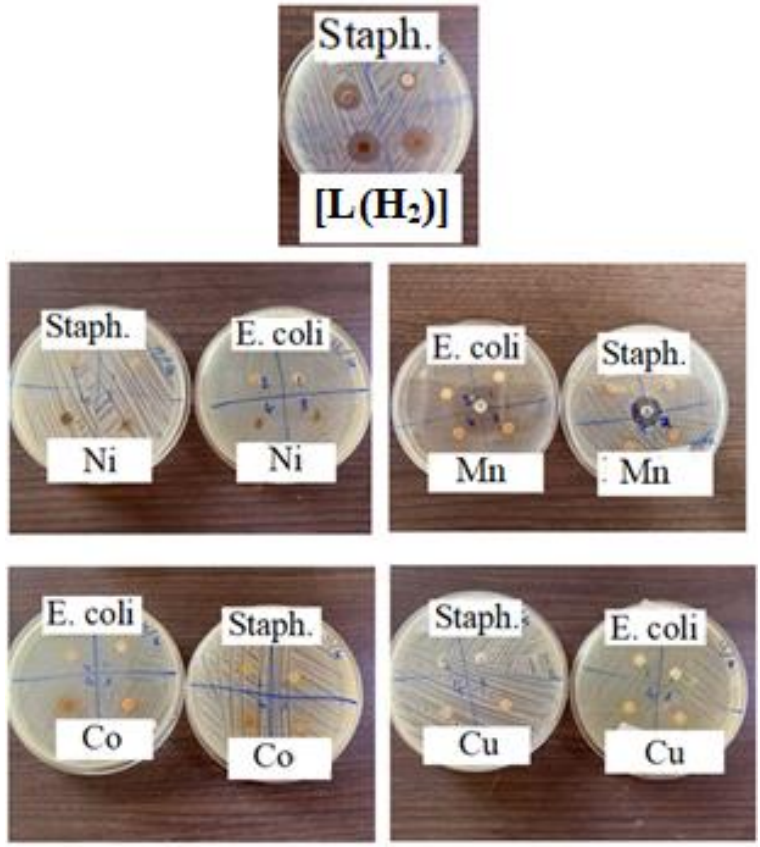

Figure 8 biological activity of derivative ligand [LH_2] and its complexes

Conclusion

The reaction of dimethylglyoxime and acetic acid with 4-aminophenol gives a new derivative ligand [LH_2]. The reaction of this ligands with metal acetates resulted in the formation of the required complex with trigonal bipyramidal geometry around Mn(II), Co(II), Ni(II), and Cu(II) ion complex with the general formula [$M(LH_2)$]. The (FT-IR) spectra of the ligands and complexes showed a new difference peaks in the FT-IR region indicating the forming compounds. The (UV-Vis) spectra of the ligands and complexes appear a new difference peaks in the visible region belongs to d-d transition type indicating the coordination with the metal ions. Magnetic moment measurements indicating the geometrical shapes of the complexes which is the trigonal bipyramidal shapes.

Acknowledgment

I appreciate my supervisor, Assistant Prof. Dr. Iman Ibrahim, for her guidance and encouragement. Many thanks for Dr. Kosrat Nazhad Dr.Bashdar Ismael and Mr.Shalaw Kamal for helping me to complete all the required measurements. I would also to thank my family who supported me to finish my thesis.

Reference

ABU-DIEF, A. M. & MOHAMED, I. M. 2015. A review on versatile applications of transition metal complexes incorporating Schiff bases. *Beni-suef university journal of basic and applied sciences,* 4**,** 119-133.

ASADI, M., SEPEHRPOUR, H. & MOHAMMADI, K. 2011. Tetradentate Schiff base ligands of 3, 4-diaminobenzophenone: Synthesis, characterization and thermodynamics of complex formation with Ni (II), Cu (II) and Zn (II) metal ions. *Journal of the Serbian Chemical Society*, 76**,** 63-74.

BAIN, G. A. & BERRY, J. F. 2008. Diamagnetic corrections and Pascal's constants. *Journal of Chemical Education,* 85**,** 532.

CHAMAYOU, A.-C., LÜDEKE, S., BRECHT, V., FREEDMAN, T. B., NAFIE, L. A. & JANIAK, C. 2011. Chirality and diastereoselection of Δ/Λ-configured tetrahedral zinc complexes through enantiopure Schiff base complexes: combined vibrational circular dichroism, density functional theory, 1H NMR, and X-ray structural studies. *Inorganic Chemistry,* 50**,** 11363-11374.

DIAB, M., MOHAMED, G. G., MAHMOUD, W., EL-SONBATI, A., MORGAN, S. M. & ABBAS, S. 2019. Inner metal complexes of tetradentate Schiff base: Synthesis, characterization, biological activity and molecular docking studies. *Applied Organometallic Chemistry,* 33**,** e4945.

EL-BORAEY, H. A., EL-SALAMONY, M. A. & HATHOUT, A. A. 2016. Macrocyclic [N5] transition metal complexes: synthesis, characterization and biological activities. *Journal of Inclusion Phenomena and Macrocyclic Chemistry,* 86**,** 153-166.

FATIMA, T., RAUF, M. K., ANWAR, M. S., RAHEEL, A., TAHIR, M. N. & ASHFAQ, M. 2020. Synthesis, characterization and magnetic studies for a series of compounds having a trinuclear bimetallic Cu_2 (II)/Ln (III) system. *Polyhedron,* 186**,** 114605.

GEARY, W. J. 1971. The use of conductivity measurements in organic solvents for the characterisation of coordination compounds. *Coordination Chemistry Reviews,* 7**,** 81-122.

GEETE, A., SHRIVASTAVA, B. & MISHRA, A. 2020. XRD Study of Cobalt [Co (ii)] Complexes Synthesized with Ligands of Aniline/Toluidine Dithiocarbamate. *vacuum,* 21**,** 24.

IBRAHEEM, I. H., ALIAS, M. F. & ALI, D. U. 2016. Synthesis and Bacterial Evaluation of The V (IV), Cr (III), Fe (III) and Co (II) Ions Complexes with Mixed Ligands (2-hydroxybenzaldine)-4-Aminoantipyrine and 8-Hydroxyquinoline. *Al-Nahrain Journal of Science,* 19**,** 9-17.

LAMANI, S. S., KOTRESH, O., A PHANIBAND, M. S. & C KADAKOL, J. 2009. Synthesis, characterization and antimicrobial properties of schiff bases derived from condensation of 8-formyl-7-hydroxy-4-methylcoumarin and substituted triazole derivatives. *E-Journal of Chemistry,* 6**,** S239-S246.

LIAO, Z.-R., ZHENG, X.-F., LUO, B.-S., SHEN, L.-R., LI, D.-F., LIU, H.-L. & ZHAO, W. 2001. Synthesis, characterization and SOD-like activities of manganese-containing complexes with N, N, N′, N′-tetrakis (2′-benzimidazolyl methyl)-1, 2-ethanediamine (EDTB). *Polyhedron,* 20**,** 2813-2821.

MAURYA, R., PATEL, P. & SUTRADHAR, D. 2003. Synthesis, magnetic, thermal, and spectral studies of some chelates of Cu (II), Ni (II), Zn (II), Co (II), Mn (II), Sm (III), and Th (IV) involving aroylhydrazones derived from isonicotinic acid hydrazide and 2-furyl methyl and 2-thienyl methyl ketone. *Synthesis and reactivity in inorganic and metal-organic chemistry,* 33**,** 1857-1876.

MELTZER, V., OANCEA, P., STANCULESCU, I. & PINCU, E. 2021. Physico-chemical characterization of solid state reaction between terephtalaldehyde and p-aminophenol. *Rev. Roum. Chim,* 66**,** 273-280.

MONDAL, I., FRONTERA, A. & CHATTOPADHYAY, S. 2021. On the importance of RH 3 C··· N tetrel bonding interactions in the solid state of a dinuclear zinc complex with a tetradentate Schiff base ligand. *CrystEngComm,* 23**,** 3391-3397.

MONFARED, H. H., VAHEDPOUR, M., YEGANEH, M. M., GHORBANLOO, M., MAYER, P. & JANIAK, C. 2011. Concentration dependent tautomerism in green [Cu (HL 1)(L 2)] and brown [Cu (L 1)(HL 2)] with H 2 L 1=(E)-N′-(2-hydroxy-3-methoxybenzylidene) benzoylhydrazone and HL 2= pyridine-4-carboxylic (isonicotinic) acid. *Dalton Transactions,* 40**,** 1286-1294.

MUSHTAQUE, M., AVECILLA, F., PINGALE, S. S., KAMBLE, K. M., YAB, Z. & RIZVI, M. M. A. 2017. Computational and experimental studies of 4-thiazolidinone-cyclopropyl hybrid. *Journal of Molecular Liquids,* 241**,** 912-921.

NUMAN, A. T., SANAK, K. A., ATIYAH, E. M. & SADIQ, S. A. 2015. Synthesis and characterization of new bidentate chalcone ligand type (NO) and its Mn II, Co II, Ni II and Cu II complexes with study of their antibacterial activity. *Diyala Journal For Pure Sciences,* 11**,** 19-30.

PIMSIN, N., KONGSANAN, N., KEAWPROM, C., SRICHAROEN, P., NUENGMATCHA, P., OH, W.-C., AREEROB, Y., CHANTHAI, S. & LIMCHOOWONG, N. 2021. Ultratrace Detection of Nickel (II) Ions in Water Samples Using Dimethylglyoxime-Doped GQDs as the Induced Metal Complex Nanoparticles by a Resonance Light Scattering Sensor. *ACS omega,* 6**,** 14796-14805.

POPESCU, M.-C., FROIDEVAUX, J., NAVI, P. & POPESCU, C.-M. 2013. Structural modifications of Tilia cordata wood during heat treatment investigated by FT-IR and 2D IR correlation spectroscopy. *Journal of Molecular Structure,* 1033**,** 176-186.

SHARMA, P., BHALE, J., MISHRA, A. & MALVIYA, P. Synthesis and X-ray diffraction study of some nickel (II) complexes of urea and thiourea. Journal of Physics: Conference Series, 2014. IOP Publishing, 012044.

SICKERMAN, N. S., PARK, Y. J., NG, G. K.-Y., BATES, J. E., HILKERT, M., ZILLER, J. W., FURCHE, F. & BOROVIK, A. 2012. Synthesis, structure, and physical properties for a series of trigonal bipyramidal M II–Cl complexes with intramolecular hydrogen bonds. *Dalton Transactions,* 41**,** 4358-4364.

SINGH, G., KAUR, J. D., SAINI, A., DEVI, A. & SATIJA, P. 2021. Synthesis, characterization and UV–visible study of schiff base-acetylene

functionalized organosilatrane receptor for the dual detection of Zn2+ and Co2+ ions. *Inorganica Chimica Acta*, 525**,** 120465.

ZAKI, M., FADDA, A., SAMIR, K. & AMER, F. 2006. Nitriles in organic synthesis: A convenient route to some heterocycles incorporating a benzothiazole moiety. *Phosphorus, Sulfur, and Silicon and the Related Elements*, 181**,** 1815-1823.